

| | |
|--------------------------------|---------------------------------------------------------------------------------------------------------------------------------------------------------------------------------------------------------------------------------------------------------------------------------------------------------------------------|
| Titre: Title: | The structural amphiphilicity of cellulose nanocrystals characterized from their cohesion parameters |
| Auteurs: Authors: | Charles Bruel, Jason R.Tavares, Pierre J.Carreau et Marie-Claude Heuzey |
| Date: | 2019 |
| Type: | Article de revue / Journal article |
| Référence: Citation: | Bruel, C., Tavares, J. R., Carreau, P. J. & Heuzey, M.-C. (2019). The structural amphiphilicity of cellulose nanocrystals characterized from their cohesion parameters. <i>Carbohydrate Polymers</i> , 205, p. 184-191. doi: 10.1016/j.carbpol.2018.10.026 |



Document en libre accès dans PolyPublie

Open Access document in PolyPublie

| | |
|---------------------------------------------------|-------------------------------------------------------------------------------------------|
| URL de PolyPublie: PolyPublie URL: | https://publications.polymtl.ca/4111/ |
| Version: | Version finale avant publication / Accepted version Révisé par les pairs / Refereed |
| Conditions d'utilisation: Terms of Use: | CC BY-NC-ND |



Document publié chez l'éditeur officiel

Document issued by the official publisher

| | |
|---------------------------------------------|-----------------------------------------------------------------------------------------------------------|
| Titre de la revue: Journal Title: | Carbohydrate Polymers |
| Maison d'édition: Publisher: | Elsevier |
| URL officiel: Official URL: | https://doi.org/10.1016/j.carbpol.2018.10.026 |
| Mention légale: Legal notice: | |

**Ce fichier a été téléchargé à partir de PolyPublie,
le dépôt institutionnel de Polytechnique Montréal**

This file has been downloaded from PolyPublie, the
institutional repository of Polytechnique Montréal

<http://publications.polymtl.ca>

The structural amphiphilicity of cellulose nanocrystals characterized from their cohesion parameters

Charles Bruel¹, Jason R. Tavares, Pierre J. Carreau, Marie-Claude Heuzey²

*Research Center for High Performance Polymer and Composite Systems (CREPEC),
Chemical Engineering Department, Polytechnique Montreal, P.O. Box 6079, Stn
Centre-Ville, Montreal, QC H3C 3A7, Canada.*

Abstract

Cellulose nanocrystals (CNCs), usually considered as isotropically polar nanoparticles, are sheet-like crystalline assemblies of cellulose chains. Here, we link the anisotropy of the CNC structure to an amphiphilic behavior in suspension. The Hansen solubility parameters (HSP: δ_D ; δ_P ; δ_H) of wood-based H₂SO₄-hydrolyzed CNCs were measured from sedimentation tests in a wide set of 59 solvents and binary mixtures. Two sets of cohesion parameters corresponding to a polar surface $(18.1; 20.4; 15.3) \pm (0.5; 0.5; 0.4)$ MPa^{1/2} and to a mildly non-polar one $(17.4; 4.8; 6.5) \pm (0.3; 0.5; 0.6)$ MPa^{1/2} were determined, with respective solubility radii of 7.8 and 2.1 MPa^{1/2}. The polar sphere is thought to correspond to the (110)&(1 $\bar{1}$ 0) surfaces of cellulose I $_{\beta}$ nanocrystals, while the smaller non-polar sphere is coherent with the exposure of (200) surfaces. The HSP graph provides new insights on the amphiphilic nature of CNCs and **a mapping of their chemical affinity for solvents and polymer matrices.**

Keywords:

cellulose nanocrystals, surface properties, structure-property relationships, **chemical affinity**, amphiphilicity, Hansen solubility parameters

¹charles.bruel@polymtl.ca

²marie-claude.heuzey@polymtl.ca

1. Introduction

D-glucopyranose polymerization produces, through a dehydration, polysaccharides such as starch, glycogen, dextran, and cellulose (Dufresne, 2017; French, 2017). In (1,4)-linked macromolecules, anhydroglucose rings are locked in a chair conformation where all their hydrophilic hydroxyl groups are in equatorial position while all their more hydrophobic C-H bonds are axial. For α -(1,4)-linked polysaccharides, such as dextrans, it results in an apolar behavior in solution (Dufresne, 2017), a feature famously exploited in cyclodextrins whose structure forms a cavity rich in C-H bonds that may be used to encapsulate hydrophobic chemicals (Marques, 2010), including for delivery in living organisms (Chaturvedi et al., 2011).

Although being insoluble in water, amorphous cellulose, a β -(1,4)-linked polymer of anhydroglucopyranose (Fig. 1.a&b), does not display such a marked apolarity in solution (Medronho et al., 2012; Dufresne, 2017). Its structural anisotropy, and its resulting amphiphilicity (Medronho et al., 2012), are however reflected in the crystalline networks cellulose chains form in living organisms such as plants, fungi, algae, bacteria, or tunicates (Moon et al., 2011; Hamad, 2017). From the various allomorphs (Moon et al., 2011; Dufresne, 2017), cellulose I_α (Nishiyama et al., 2003) and I_β (Nishiyama et al., 2002) are the only ones that may be found naturally in land plants (Moon et al., 2011). They both reproduce on the nanocrystal level the anisotropy of their monomeric unit. Indeed, cellulose chains assemble in sheets, parallel to the equatorial planes of the anhydroglucose rings, which then stack up to form multilayer crystalline structures, crystallites (Fig. 1.c) (Jarvis, 2003; Li & Renneckar, 2011). Intra and intersheet cohesions are respectively insured by interchain OH-O hydrogen bonds and by weaker interchain CH-O and van der Waals interactions (Jarvis, 2003; Nishiyama, 2017). The formation of these van der Waals interactions is thought to be the initial step through which cellulose chains crystallize (Cousins & Brown, 1995).

Hydrolysing cellulosic feedstocks in acidic conditions, usually with sulfuric acid, digests their amorphous and non-cellulosic contents while mostly preserving their crystalline parts (Dufresne, 2017; Moon et al., 2011; Hamad, 2017). Under harsh enough conditions, the treatment yields highly crystalline cellulose-made particles, cellulose nanocrystals (CNCs). They are hypothesized to be made of several adjacent crystallites (Uhlig et al., 2016; Ding et al., 2012, 2014) assembled with a right-handed chirality (Usov et al., 2015). Introduction of sulfate half-ester groups at CNC surface during the

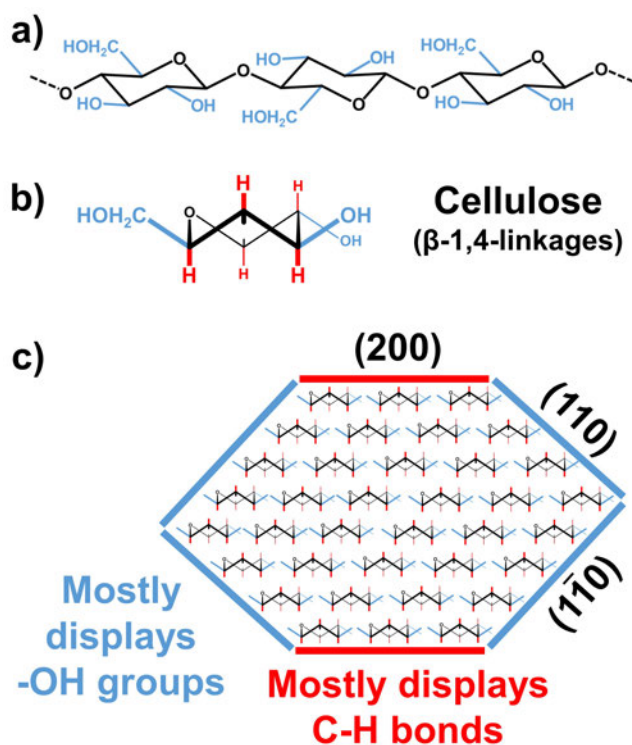


Figure 1: Anisotropy of cellulose. (a) Cellulose, a β -(1,4)-linked polymer of anhydroglucopyranose (French, 2017), has its monomeric units locked in a conformation where all their hydroxyl substituents (in blue) are in equatorial position while their C-H bonds (in red) are axial as exemplified in a profile view (b). (c) The structure of cellulose I_β crystallite reflects this anisotropy as cellulose chains are arranged in sheets held together by OH-O hydrogen bonds, which then stack-up through the formation of CH-O H-bonds and van der Waals interactions (Jarvis, 2003; Li & Rennekar, 2011). Based on Ding and Himmel’s model (Ding & Himmel, 2006), the resulting crystallite displays up to three kind of surfaces corresponding to the lattice planes (110), ($\bar{1}\bar{1}0$), and (200) of its crystalline unit. The latter displays mostly C-H bonds, while the two former are rich in hydroxyl groups.

38 hydrolysis provides them with an electrostatic stabilization upon suspension
 39 in water and with interesting self-organization properties (Liu et al., 2011;
 40 Hamad, 2017).

41 CNCs, especially sulfated ones, are usually described as polar particles,
 42 which stems from the difficulty encountered to disperse them in non-polar
 43 solvents and polymer matrices (Hamad, 2017). Although arising from exper-
 44 imental observations, this description is at odd with the amphiphilic behav-
 45 ior that can be expected from CNC anisotropic structure. Analysis of wide

46 (WAXS) and small angle X-ray scattering (SAXS) (Elazzouzi-Hafraoui et al.,
 47 2008; Sèbe et al., 2012) as well as high resolution atomic force microscopy
 48 (AFM) (Ding et al., 2006; 2012; 2014) indeed suggests that up to three kinds
 49 of lateral surfaces are displayed by the nanocrystals extracted from cellulose
 50 I_β sources (Fig. 1.c), by far the most common allomorph in higher plants
 51 –wood included (Atalla & Vanderhart, 1999; Habibi et al., 2010). Within
 52 the crystalline unit, they correspond respectively to the lattice planes (110),
 53 $(1\bar{1}0)$, and (200) (Ding & Himmel, 2006; Brown, 1996). The latter, parallel
 54 to the sheets plane, displays mostly C-H bonds, while the two former in-
 55 tersect the plane of the sheets and thus display hydroxyl groups (Fig. 1.c).
 56 Molecular dynamic simulations suggests that (110) and $(1\bar{1}0)$ surfaces have
 57 similar hydrophilicity (Heiner et al., 1998; Matthews et al., 2006) and surface
 58 energies (Yamane et al., 2006), while (200) surfaces are expected to be more
 59 hydrophobic, with higher water contact angle (Mazeau & Rivet, 2008) and
 60 lower surface energies (Yamane et al., 2006) (Table 1).

Table 1: Cellulose nanocrystal surface properties according to the lattice plane displayed.
 δ_T is the total solubility parameter. δ_D , δ_P , and δ_H are its decomposition in term of
 dispersive, polar, and hydrogen bonding components, respectively (Hansen, 2007). R_0 is
 the HSP radius.

| Lattice plane | | (110) | $(1\bar{1}0)$ | (200) |
|----------------------------------|--------------------|----------|---------------|----------|
| Surface energy ^a | mN m ⁻¹ | 155 | 155 | 92 |
| Water contact angle ^b | ° | 43 | - | 95 |
| δ_T | MPa ^{1/2} | 31.3±1.4 | | 19.2±2.7 |
| δ_D | MPa ^{1/2} | 18.1±0.5 | | 17.4±0.3 |
| δ_P | MPa ^{1/2} | 20.4±0.5 | | 4.8±0.5 |
| δ_H | MPa ^{1/2} | 15.3±0.4 | | 6.5±0.6 |
| R_0 | MPa ^{1/2} | 7.8 | | 2.1 |

^a Modeled values as calculated by Yamane et al. (2006).

^b Modeled values as calculated by Mazeau & Rivet (2008).

61 Chemically, a proof that CNCs display **hydroxyl groups rich surfaces –**
 62 **which would correspond to the (110) and $(1\bar{1}0)$ lattice planes–** may be pro-
 63 **vided easily by attempting to functionalize them (Eyley & Thielemans, 2014).**
 64 **$(1\bar{1}0)$ lattice planes have furthermore already been observed by atomic force**
 65 **microscopy on cellulose I_β samples (Kuutti et al., 1995).** The detection of un-
 66 **reactive C-H bonds rich surfaces –which would correspond to the (200) lattice**
 67 **plane–** is, however, harder to achieve. The main clue is that the display of
 68 (200) lattice planes by CNCs should result in a certain level of amphiphilic-

69 ity, as experimentally confirmed : stable suspensions of CNCs in chloroform
70 have been reported (Yu & Qin, 2012; Yu et al., 2012). This mildly non-polar
71 solvent may also form inclusions in cellulose I fibers (Wade & Creely, 1974).
72 It is worth noting that not every work reports a good dispersion in chloro-
73 form (Yoo & Youngblood, 2016; Petersson et al., 2007) and it remains to
74 be seen whether this divergence has to be attributed to differences in feed-
75 stock, hydrolysis conditions, or protocol of dispersion, such as the intensity of
76 the ultrasonication for instance. Other hydrophobic interactions of cellulose
77 include those with cellulases (Himmel et al., 2007; Mazeau & Rivet, 2008)
78 and congo red (Mazeau & Wyszomirski, 2012; Conley et al., 2017b,a) whose
79 aromatic parts are both thought to adsorb primarily on the (200) surfaces.

80 Although these preliminary results point toward a chemical influence of
81 (200) surfaces for some CNC suspensions, thus conforming WAXS, SAXS,
82 and AFM observations, none of them really isolate their potential contribu-
83 tion from the stronger influence of the (110) and (1 $\bar{1}$ 0) surfaces.

84 In this work, we apply a thermodynamic approach based on the Hansen
85 solubility parameters (HSP) and on sedimentation tests using 59 solvents and
86 binary mixtures, to isolate experimentally the influence of the hydrophobic
87 (200) surfaces from the predominant one of the more hydrophilic (110) and
88 (1 $\bar{1}$ 0) surfaces (as reported in Table 1). These investigations result into a
89 mapping of CNC affinity for common solvents and polymers. The identifica-
90 tion of an amphiphilic behavior for the nanocrystals establishes a direct link
91 between their structure and their surface properties.

92 2. Materials and methods

93 2.1. Materials

94 CNCs, provided by Celluforce (Montreal, QC, Canada) as a spray-dried
95 powder, were obtained from Kraft wood pulp by a sulfuric acid hydrolysis
96 treatment followed by a neutralization with sodium hydroxide (NaOH). Pre-
97 vious work from our team on CNCs from the same batch demonstrated that
98 these particles are in average ~ 165 nm long and ~ 13 nm wide with a sulfur
99 content equivalent of 3.4 sulfate half ester (O-SO₃H) per 100 anhydroglucose
100 units (Beuguel et al., 2018b). **The X-ray diffractogram is typical of I β cellu-**
101 **lose (Elazzouzi-Hafraoui et al., 2008; Sèbe et al., 2012) and** the crystallinity
102 index was found to be of 81 %.

103 To obtain the dimensions of the CNCs the following procedure was ap-
104 plied (Beuguel et al., 2018b). A drop of a sonicated water suspension of

105 CNCs, diluted at $10 \mu\text{g}_{\text{CNCs}} \text{mL}_{\text{water}}^{-1}$, was deposited on a copper TEM grid
106 covered by a 5 to 6 nm-thick layer of pure carbon. Average dimensions, with
107 standard deviations in the range of $\pm 10\%$, were obtained from measurements
108 of over 100 particles performed on transmission electronic microscopy (TEM)
109 micrographs obtained at 200 kV with a bright field imaging Jeol JEM 2100F
110 (Beuguel et al., 2018b). The sulfur content was measured from X-Ray energy
111 dispersive spectroscopy (EDX) analysis performed on the CNC spray-dried
112 powder with a Tabletop Hitachi TM3030+ scanning electron microscope.
113 Scanning of three samples on different locations, for a total of ten scans,
114 yielded a sulfur over carbon (S/C) atomic ratio of 0.0057 with a standard
115 deviation of ± 0.0005 (Beuguel et al., 2018b). The oxygen over carbon (O/C)
116 atomic ratio was of 0.79 ± 0.02 , very close to the theoretical value of 0.83
117 for cellulose, and is indicative of a high level of purity for the nanocrystals
118 (Siqueira et al., 2010). The CNC crystallinity was measured through X-ray
119 diffraction (XRD) with a X'pert instrument (Philips) operating with Cu $K\alpha$
120 radiations (wavelength of 0.1542 nm generated at 50 kV with a current of
121 40 mA. Scan type was continuous with an angle 2θ varying from 5.01° to
122 49.99° with steps of 0.02° and a scan time of 1 s per step. The crystallinity
123 index, IC , was measured as $IC = 1 - I_{\text{AM}}/I_{200}$, according to Segal's empirical
124 method (Segal et al., 1959). I_{AM} and I_{200} are the intensities of the amorphous
125 peak ($2\theta = 18.85^\circ$) and of the peak corresponding to the (200) lattice planes
126 ($2\theta = 23.01^\circ$), respectively.

127 Organic solvents employed were purchased from commercial suppliers at
128 high purity grade (purity $> 99\%$, see Table A.1). The only exceptions are
129 ethanol, used in its denatured form (purity of $\sim 95\%$), and d-limonene (purity
130 of $\sim 96\%$), as higher purity grades of d-limonene are generally not available
131 commercially. Distilled water was employed. Binary mixtures were prepared
132 by mixing pure solvents. Densities and viscosities of solvents and mixtures
133 at 25°C were obtained by averaging experimental values reported in the
134 specialized literature (Tables A.1&A.2).

135 2.2. Sedimentation tests

136 2.2.1. Protocol

137 10 mL of the different solvents and binary mixtures were added to 0.1 g
138 of CNCs in a glass vials of radius 2.1 cm. An ultrasonic probe (Cole-Parmer)
139 operating at a frequency of 20 kHz with a CV334 converter and a tapered
140 microtip was used to disperse the CNCs. The treatment had a power of
141 $\sim 25\text{ W}$ and was applied with a pulse cycle ON-OFF of 5 s-2 s for a total

142 energy of $10,000 \text{ J g}_{\text{CNCs}}^{-1}$. Previous experimentation demonstrated that such a
 143 treatment do not result into desulfation of the CNCs (Beuguel et al., 2018b).
 144 The vials were placed in an ice bath to avoid any overheating during the
 145 ultrasonication. CNC suspensions ($10 \text{ mg}_{\text{CNCs}} \text{ mL}_{\text{solvent}}^{-1}$) were then allowed
 146 to rest at 25°C for a relative sedimentation time, $RST = 1.18 \times 10^{11} \text{ s}^2\text{m}^{-2}$.
 147 Calculated with Eq. 1 (Hansen, 2007), it corresponds for instance to an
 148 absolute sedimentation time, t_{sed} , of 12.1 h in acetone, 48.0 h in water, or
 149 1140 h in ethylene glycol (Tables A.1&A.2). Once the time of sedimentation
 150 had elapsed, three kinds of qualitative behaviors were observed for CNC
 151 sedimentation. Graded on a scale from best, 2, to worst, 0, they correspond
 152 respectively to: 2- a suspension without formation of any sediment (as shown
 153 in Fig. 2.a for DMSO), 1- a turbid suspension in which a sediment is formed
 154 (dichloromethane), and 0- all remaining cases in which a sediment is formed
 155 and the suspension is clear enough for text to be read through (toluene).
 156 The only exception to the aforementioned protocol is the sedimentation in
 157 triethanolamine, which was interrupted after a RST of $1.18 \times 10^{10} \text{ s}^2\text{m}^{-2}$ (10%
 158 of the standard RST). Due to the very high viscosity of triethanolamine, it
 159 corresponds to a time of sedimentation t_{sed} of 4100 h. Its behavior is clearly
 160 that of a 0-grade solvent (Fig. A.1).

$$t_{\text{sed}} = RST \frac{\eta_{\text{solv}}}{\rho_{\text{CNCs}} - \rho_{\text{solv}}} \quad (1)$$

161 2.2.2. RST calibration

162 Sulfating CNCs provides them with surface charges, generating electro-
 163 static stabilization. It is a kinetic effect: the thermodynamically favored
 164 outcome of a colloidal suspension is the coagulation of the particles (Kron-
 165 berg et al., 2014). For electrostatic stabilization to manifest, there has to
 166 be dissociation between the negatively charged CNCs and their counter-ions,
 167 an outcome favored in solvents whose dielectric constants, ϵ_{solv} , are high
 168 (Kronberg et al., 2014). HSP characterization is a thermodynamic approach
 169 and a RST of $1.18 \times 10^{11} \text{ s}^2\text{m}^{-2}$ was selected following a calibration aimed at
 170 minimizing the influence of such kinetic effects on the sedimentation results.

171 At low RST , sedimentation results were strongly correlated with the di-
 172 electric constants of the solvents (Table A.1). Quickly, a discrimination how-
 173 ever appears among highly dielectric solvents and, at a RST of $5.9 \times 10^{10} \text{ s}^2\text{m}^{-2}$,
 174 we were already able to hint “good” solvents from “poor” ones independently
 175 of their dielectric constant. At $RST = 1.18 \times 10^{11} \text{ s}^2\text{m}^{-2}$, results are no

176 longer correlated with the dielectric constants. Highly dielectric solvents
177 like methanol ($\epsilon_{\text{solv}}=33.0$), ethylene glycol (41.4), DMF (38.3), or propylene
178 carbonate (66.1) received the grade 0, while DMSO (47.2) or ethanolamine
179 (31.9) are at 2. The state of sedimentation at $RST = 1.18 \times 10^{11} \text{ s}^2\text{m}^{-2}$ was
180 found to be meta-stable as increasing the RST beyond $1.18 \times 10^{11} \text{ s}^2\text{m}^{-2}$ no
181 longer affects the results. Vials were kept for months and in volatile media
182 such as chloroform and dichloromethane, the solvent was fully evaporated
183 before any significant change in the suspension turbidity could be observed.
184 It does not mean that the electrostatic stabilizing effect is no longer felt
185 at $RST = 1.18 \times 10^{11} \text{ s}^2\text{m}^{-2}$, but that electrostatic stabilization alone is no
186 longer sufficient to prevent sedimentation at this point. For particles to re-
187 main in suspension at high RST , and whatever the level of electrostatic
188 stabilization, there has to be a certain level of chemical affinity. It is this
189 chemical affinity that the HSP analysis seeks to capture.

190 *2.3. Thermodynamic approach - Hansen solubility parameters*

191 *2.3.1. Background*

192 Initially developed to address the issue of the dispersibility of the vari-
193 ous components of paints, solubility -or cohesion- parameters theory aims at
194 quantifying the cohesive energy density (taken equal to δ_{T}^2 , MPa) between a
195 chemical and its neighboring media (Hildebrand & Scott, 1950, 1962; Hansen,
196 2007). Hansen proposed to split the total cohesion parameter, δ_{T} , into its
197 three main components resulting from the London dispersion forces (δ_{D}),
198 the dipole-dipole interactions (δ_{P}), and hydrogen bonding interactions (δ_{H})
199 (Hansen 1967a,b, 2007; Hansen & Skaarup, 1967). The linearity of the de-
200 composition in terms of energies means that δ_{T} square may then be written
201 as the sum of the squared HSP (Eq. 2). In the HSP theory, every chem-
202 ical may be represented by a triplet (δ_{D} , δ_{P} , δ_{H}), and then be plotted in
203 a 3 dimensional graph (Hansen, 2007). HSP values of solvents may be de-
204 termined directly experimentally or estimated by group contribution meth-
205 ods and are now tabulated, alongside those of many commodity polymers
206 (Hansen, 1967b, 2007; Abbott et al., 2018). Gardebjer et al. (2016) used
207 one of these group contribution methods to estimate the HSP of cellulose's
208 repeating unit, cellobiose. They computed a value of $(\delta_{\text{D}}, \delta_{\text{P}}, \delta_{\text{H}}) = (16.3;$
209 $16.2; 20.7) \text{ MPa}^{1/2}$ and assumed it to be the HSP values of CNCs (Gardebjer
210 et al., 2016). Although it provided a quick and easy estimate, the method
211 is unsatisfactory as it does not take into account the fact that polymer HSP
212 are almost systematically greater than those of their repeating units, nor the

213 fact that crystallinity may greatly affect HSP values (Hansen, 2007; Abbott
 214 et al., 2018). Unknown HSP may be determined more accurately through an
 215 indirect approach. Affinity tests between the material and various solvents
 216 are conducted with the idea that, “like seeking like”, the stronger are the
 217 interactions the shorter is the distance, R_a ($\text{MPa}^{1/2}$, Eq. 3), between their
 218 respective Hansen solubility parameters (Hansen, 2007). “Good” solvents,
 219 where the “goodness” may be assigned quantitatively (e.g. maximum solu-
 220 bility) or qualitatively (e.g. suspension turbidity or swelling behavior), thus
 221 describe a sphere of radius R_0 ($\text{MPa}^{1/2}$), whose center corresponds to the
 222 unknown’s HSP (Hansen, 2007). The set of solvents may be completed by
 223 mixtures (Machui et al., 2012), Their HSP ($\delta_{D,\text{mix}}$; $\delta_{P,\text{mix}}$; $\delta_{H,\text{mix}}$) were calcu-
 224 lated through Eq. 4 (Hansen, 2007), in which ($\delta_{D,i}$; $\delta_{P,i}$; $\delta_{H,i}$) are the HSP
 225 values of the constituent i and Φ_i its volume fraction; n is the total number
 226 of solvents in the mixture.

$$\delta_T^2 = \delta_D^2 + \delta_P^2 + \delta_H^2 \quad (2)$$

$$R_a^2 = 4(\delta_{D,1} - \delta_{D,2})^2 + (\delta_{P,1} - \delta_{P,2})^2 + (\delta_{H,1} - \delta_{H,2})^2 \quad (3)$$

$$\delta_{D,\text{mix}} = \sum_{i=1}^n \Phi_i \delta_{D,i}; \quad \delta_{P,\text{mix}} = \sum_{i=1}^n \Phi_i \delta_{P,i}; \quad \delta_{H,\text{mix}} = \sum_{i=1}^n \Phi_i \delta_{H,i} \quad (4)$$

227 Our set of solvents was selected based on their position in the HSP graph
 228 to maximize the coverage and based on the uncertainty of the solvents’ HSP
 229 coordinates. Indeed, the indirect method of HSP determination for an un-
 230 known compound is no more precise than that of the solvents that are em-
 231 ployed to perform the characterization. Historically, HSP coordinates were
 232 determined experimentally for a set of 90 common solvents, from which group
 233 contribution models have been derived (Hansen, 2007). Nowadays, and based
 234 on these group contribution methods, HSP of thousands of solvents have
 235 been calculated (Hansen, 2007; Abbott et al., 2018). When we selected our
 236 27 pure solvents, we aimed at picking them from the list of the 90 experimen-
 237 tally confirmed solvents. Exceptions to the list are ethyl benzoate, heptane,
 238 d-limonene, triethanolamine, and water. Water, with its three sets of HSP,
 239 is a special case (see Hansen 2007). Heptane, being purely dispersive, has a
 240 low uncertainty (uncertainty arises mostly from the calculation of the polar
 241 and hydrogen-bonding components: δ_P and δ_H , respectively) (Abbott et al.,
 242 2018). Ethyl benzoate, d-limonene, and triethanolamine HSP values have

243 been calculated, rather than empirically determined, inducing a greater un-
 244 certainty. They were nonetheless selected for their interesting position in the
 245 HSP graph.

246 2.3.2. HSP analysis

247 HSP analysis was performed with the software HSPiP (Abbott et al.,
 248 2018). HSP values of pure solvents, binary mixtures, and polymers, were
 249 extracted from the HSPiP database (Abbott et al., 2018) and are respectively
 250 provided in Tables A.1, A.2, and A.3.

251 For the sphere fitting, we considered both grade 1 and grade 2-solvents
 252 (and mixtures) to be “good” and grade 0-ones to be “poor”. The algorithm of
 253 the software maximizes the function *FIT* described below (Eq. 6) (Hansen,
 254 2007; Abbott et al., 2018). The ideal result is a sphere of center $(\delta_{D,s}$; $\delta_{P,s}$
 255 ; $\delta_{H,s})$ and of radius R_0 that contains all the “good” solvents and mixtures
 256 while excluding any “poor” ones. A solvent/mixture is located in the sphere
 257 if its distance to the sphere’s center, R_a (Eq. 2), is smaller than or equal to
 258 R_0 . It corresponds to a reduced energy difference $RED \leq 1$ (Eq. 5).

$$RED = R_a/R_0 \quad (5)$$

259 The quality of the fitting may be assessed through the *FIT* value and
 260 through the uncertainty on the $(\delta_{D,s}$; $\delta_{P,s}$; $\delta_{H,s})$ coordinates (Hansen, 2007;
 261 Abbott et al., 2018). *FIT* (Eq. 6) is a desirability function (Hansen, 2007)
 262 that provides information about the quality of the fit on the m solvents tested
 263 : indeed, a “poor” solvent/mixture located inside a sphere ($RED \leq 1$) or a
 264 “good” one located outside ($RED > 1$) induces a penalty on the *FIT* coeffi-
 265 cient. The better the fit, the closest *FIT* will be from 1.0 ($FIT \leq 1.0$). The
 266 uncertainty “ $\pm(\Delta\delta_{D,s}; \Delta\delta_{P,s}; \Delta\delta_{H,s})$ ” provides information on the tightness
 267 of the HSP sphere core’s position. Values in the range of ± 0.25 - 0.50 MPa^{1/2}
 268 are indicative of a very good fit and of a tight core, while a poor fit will
 269 result in uncertainties in the range of ± 1 MPa^{1/2} (Abbott et al., 2018). It is
 270 possible to have a tight core for two parameters and a loose one for the last,
 271 meaning that there is a lack of data points in that direction (Abbott et al.,
 272 2018). It has to be noted that fitting a sphere on less than 4-5 good solvents
 273 necessarily leads to an uncertainty that may not be reflected in the *FIT*
 274 value nor in the “ $\pm(\Delta\delta_{D,s}; \Delta\delta_{P,s}; \Delta\delta_{H,s})$ ”. The existence of an uncertainty
 275 means that results obtained in running several times the algorithm on the
 276 same data differ slightly. Results reported here are those corresponding to

277 the highest FIT value and the lowest uncertainty over at least 10 runs of the
 278 fitting algorithm. The values were overall very stable between the different
 279 fits with variations in the range of 0.001 for FIT and of $\sim 0.05 \text{ MPa}^{1/2}$ for
 280 the different uncertainties: “ $\pm(\Delta\delta_{D,s}; \Delta\delta_{P,s}; \Delta\delta_{H,s})$ ”.

$$FIT = \left(\prod_{i=1}^m A_i \right)^{1/m}$$

For “good” solvents inside a sphere : $A_i = 1$ (6)

For “poor” solvents outside a sphere : $A_i = 1$

For “good” solvents outside a sphere : $A_i = e^{+(R_0-R_a)}$

For “poor” solvents inside a sphere : $A_i = e^{+(R_a-R_0)}$

281 3. Results and discussion

282 Considering both grade 2 and 1 as “good” solvents, two distinct regions of
 283 preferential dispersibility may clearly be distinguished. The first is in the po-
 284 lar region of the graph (high δ_P and δ_H , Fig. 2.c) and contains all of the grade
 285 2 solvents: dimethylsulfoxide (DMSO), formamide, water, and ethanolamine.
 286 The area delimited by these solvents is bordered by 0-grade ones like tri-
 287 ethanolamine, propylene carbonate, N,N-dimethylformamide, or acetone. A
 288 second distinct region may then be distinguished in the mildly non-polar
 289 region (intermediate δ_P and δ_H) where chloroform and dichloromethane are
 290 classified as grade 1 and stand alone surrounded by poor solvents. This
 291 behavior, with two distinct regions, is expected in the HSP theory for am-
 292 phiphilic species such as particles or block copolymers for instances (Hansen,
 293 2007). In this configuration, two HSP spheres, which correspond to the dif-
 294 ferent affinities of the chemical, may be drawn.

295 For a better HSP fit, sedimentation tests were performed for binary mix-
 296 tures of DMSO + acetone, toluene, and methanol, and binary mixtures of
 297 formamide + methanol and 1-propanol. Results obtained with binary mix-
 298 tures validate our scale of dispersibility as the “goodness” of a grade 2 solvent
 299 like DMSO decreases to grade 1 once 40 vol% of methanol, a grade 0 solvent,
 300 is added and then to 0 beyond 60 vol% (Fig. A.2.b&e). DMSO is known
 301 to be one of the best solvent for CNCs dispersion as it enables strong gel
 302 formation upon heating (Sojoudiasli et al., 2017).

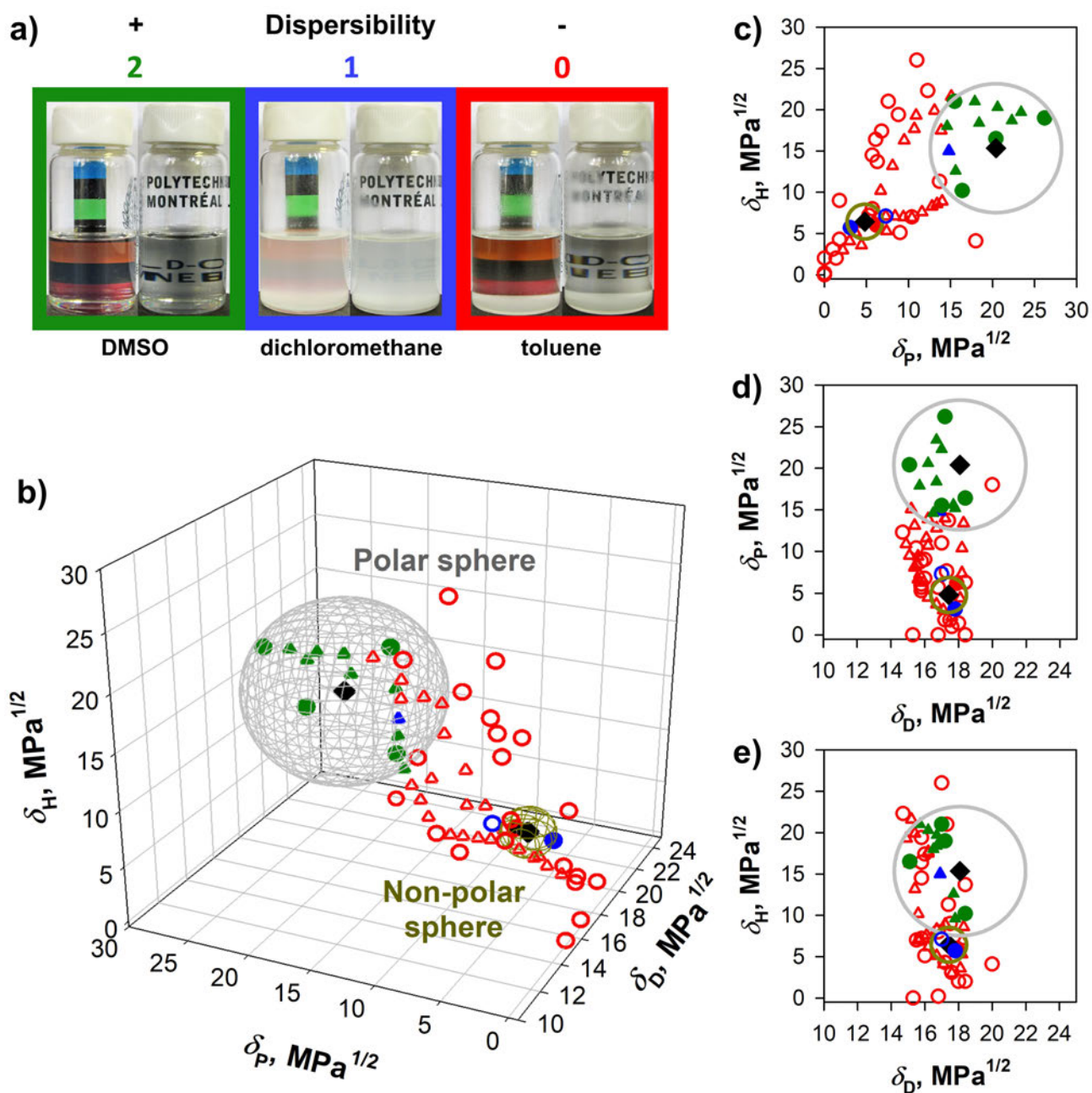


Figure 2: HSP graph of wood-based sulfuric acid-hydrolyzed CNCs. (a) CNC scale of dispersibility. Three different grades were attributed to the CNC state of dispersion, from best to worst: 2-in green-No sediment at the bottom of the vial, 1-in blue-Presence of a sediment, the suspension is too turbid to be able to read a text through, 0-in red-Presence of a sediment, the suspension is less turbid/clear. Pure solvents are represented by circles, binary mixtures by triangles, sphere centers by black diamonds. Two different spheres may be plotted : a large polar sphere ($\delta_D; \delta_P; \delta_H$) = (18.1; 20.4; 15.3) \pm (0.5; 0.5; 0.4) $\text{MPa}^{1/2}$ and another smaller sphere in the mildly non-polar region ($\delta_D; \delta_P; \delta_H$) = (17.4; 4.8; 6.5) \pm (0.3; 0.5; 0.6) $\text{MPa}^{1/2}$. Symbols located inside a sphere are full and symbols outside are empty. The HSP graph is represented in a 3-dimensional view (b), and in 2-dimensional views alongside the planes δ_H - δ_P (c), δ_P - δ_D (d), and δ_H - δ_D (e).

303 Using HSPiP (Hansen Solubility Parameters in Practice) software (Ab-
304 bott et al., 2018), it was possible to obtain a well defined sphere ($FIT =$
305 1.0, see Eq. 6) of radius $R_{0,P}=7.8 \text{ MPa}^{1/2}$ in the polar region. It includes 13
306 good solvents and mixtures while excluding any poor ones. Its center’s coordi-
307 nates ($\delta_D; \delta_P; \delta_H$) are $(18.1; 20.4; 15.3) \pm (0.5; 0.5; 0.4) \text{ MPa}^{1/2}$ for a δ_T of
308 $31.3 \pm 1.6 \text{ MPa}^{1/2}$. Having defined with precision what stands clearly for the
309 dominant affinity of CNCs, the case of chloroform and dichloromethane may
310 be addressed. These results are concordant with reports by Yu et al. of stable
311 suspensions of sulfuric acid hydrolyzed CNCs in chloroform (Yu & Qin, 2012;
312 Yu et al., 2012). A fitting in this area of the graph yields a FIT of 0.974 with
313 a sphere of radius $R_{0,P}=2.1 \text{ MPa}^{1/2}$ and centered about $(\delta_D; \delta_P; \delta_H) = (17.4;$
314 $4.8; 6.5) \pm (0.3; 0.5; 0.6) \text{ MPa}^{1/2}$. It corresponds to a δ_T of $19.2 \pm 2.7 \text{ MPa}^{1/2}$.
315 Here, the FIT value is lowered by ethyl benzoate, which is a 0-grade sol-
316 vent despite having HSP close to that of dichloromethane and chloroform.
317 It is not clear whether it highlights a limitation of the HSP method itself
318 –as we know that conformation effects for instance are not accounted for in
319 HSP theory– or a limitation of the HSP group contribution models. Ethyl
320 benzoate is indeed among the few solvents we employed whose HSP were
321 calculated without any experimental confirmation (Hansen, 2007). It may
322 thus be that the FIT value is only lowered by imprecise solvent coordinates:
323 ethyl benzoate while being plotted as inside of the non-polar sphere (Fig. 2)
324 may actually be out of it. From the 90 solvents experimentally proofed by
325 Hansen and co-workers (1967; 1967a; 1967b), and aside from chloroform and
326 dichloromethane, none is located in the area of interest. This issue cannot be
327 settled easily with the current experimental method. Fitted using only two
328 good solvents, the position of the non-polar sphere thus has to be considered
329 with caution. It however provides the first experimental estimates of CNC
330 hydrophobic surface HSP.

331 The polar sphere is considered to correspond to the HSP of the hydroxyl
332 rich (110) and ($1\bar{1}0$) surfaces. Computer simulations indeed predicts that
333 (110) and ($1\bar{1}0$) surfaces have similar surface energies (Yamane et al., 2006)
334 and hydrophilicity (Heiner et al., 1998; Matthews et al., 2006), which means
335 that they are expected to be represented by a single HSP sphere (Table 1).
336 Meanwhile, the mildly non-polar sphere is attributed to the display of (200)
337 surfaces by the nanocrystals. Their lower simulated surface energy (Yamane
338 et al., 2006) and higher modeled water contact angle (Mazeau & Rivet, 2008)
339 are indeed expected to result into a distinct HSP sphere.

340 The contrast between the better fit and wider radius of the polar sphere

341 and the lesser ones of the non-polar sphere is coherent with the fact that
 342 sulfuric acid hydrolyzed CNCs have been reported to exhibit experimentally
 343 a predominant polar and hydrophilic behavior. HSP of the polar sphere are
 344 furthermore very close to those obtained for the chemical accessibility of cel-
 345 lulose : $(\delta_D; \delta_P; \delta_H) = (19.09; 15.77; 15.29) \pm (0.15; 0.25; 0.30) \text{ MPa}^{1/2}$
 346 (Hansen & Björkman, 1998; Larsson & Johns, 1988; Minhas & Robertson,
 347 1967). These are calculated from the ability of different solvents to swell
 348 cotton-based I_α cellulose pulp. Swelling increases the active surface area of
 349 the pulp by increasing hydroxyl group accessibility, the amount of which is
 350 quantified chemically through a thallation of the -OH functions (Minhas &
 351 Robertson, 1967). The only significant deviation lies in δ_P , the polar compo-
 352 nent, that is increased by $+4.6 \text{ MPa}^{1/2}$ from the chemical accessibility of cellu-
 353 lose HSP to our polar sphere’s results. Slight variations in δ_D and δ_H , coupled
 354 to a sharp increase in δ_P are coherent with the effect of surface sulfatation
 355 based on the predictions of HSP group contributions (Stefanis & Panayiotou,
 356 2008). The δ_P increase for CNCs with respect to the cotton-based pulp is
 357 thus attributed to the introduction of sulfate groups on the hydroxyl groups
 358 of the nanocrystal surfaces during the sulfuric acid hydrolysis (Hamad &
 359 Hu, 2010; Hamad, 2017). Part of this variation is also probably imputable
 360 to the difference in wettability between I_α and I_β hydroxyl-rich surfaces, al-
 361 though simulations predict very similar surface energies with 154 mN m^{-1}
 362 and 155 mN m^{-1} , respectively (Yamane et al., 2006).

363 It is worth noting that this shift of $+4.6 \text{ MPa}^{1/2}$ in δ_P reduces the HSP
 364 distance of CNCs with water from $\sim 9.3 \text{ MPa}^{1/2}$ to $\sim 6.1 \text{ MPa}^{1/2}$, which may
 365 be able to partly explain the increased affinity of sulfated CNCs for water.
 366 As contact angles have usually been found experimentally to be positively
 367 correlated with HSP distance (Hansen, 2007), this finding is also coherent
 368 with the water contact angle value obtained by simulation by Mazeau &
 369 Rivet (2008). The 43° of the (110) surface corresponds to a HSP distance
 370 of $\sim 6.1 \text{ MPa}^{1/2}$, while the 95° of the (200) surface corresponds, based on our
 371 results, to a HSP distance of $\sim 19.1 \text{ MPa}^{1/2}$.

372 From our knowledge of the CNC structure, it is thus possible to assign
 373 each of the spheres to a lattice plane, which enables us for the first time to
 374 estimate the amphiphilicity of wood-based sulfated CNCs. Our results also
 375 highlight the limitations of group contribution methods to estimate cellulose
 376 nanocrystal HSP. Given that they do not take into account conformation
 377 effects, computations by Gardebjer et al. (2016) were not able to predict
 378 a second non-polar sphere for CNCs. If we compare their results to those

379 of our polar sphere, they also underestimate δ_D and δ_P by $1.7 \text{ MPa}^{1/2}$ and
380 $4.2 \text{ MPa}^{1/2}$, respectively, which is not unexpected when HSP of a polymer
381 are compared to those of its repeating unit (Hansen, 2007). The hydrogen
382 bonding component, δ_H , was underestimated by $5.4 \text{ MPa}^{1/2}$ (Gardebjer et al.,
383 2016). It may probably be attributed to the fact that the influence of the
384 -OH groups of cellulose is hindered by their involvement in the crystalline
385 network of CNCs (Jarvis, 2003; Djahedi et al., 2016).

386 The amphiphilicity of cellulose chains has recently been advanced as a
387 key-factor to explain the low solubility of cellulose chains in polar solvents
388 (Medronho et al., 2012). This parameter was not considered by Hansen &
389 Björkman (1998) when they worked on wood ultrastructure and cellulose
390 affinity. While Fig. 2 provides experimental evidence for this amphiphilic-
391 ity, we believe that due to the high dependency of HSP with conformation
392 effects, such as those induced by crystallinity (Hansen, 2007; Abbott et al.,
393 2018), any extrapolation from crystalline to amorphous cellulose has to be
394 considered with great caution. Our interest in HSP instead lies in their abil-
395 ity to represent in a same graph –thus enabling comparisons– chemicals of
396 very different scales, from solvents to polymers, (nano)particles, and macro-
397 scale surfaces. Determining HSP of cellulose nanocrystals, based on their
398 behavior in a set of solvents, may thus provide information about their affin-
399 ity for polymer matrices. HSP of some common polymer matrices, such
400 as poly(vinyl alcohol) (PVOH), poly(lactic acid) (PLA), poly(ethylene gly-
401 col) (PEG), poly(methyl methacrylate) (PMMA), poly(ethylene) (PE), and
402 poly(propylene) (PP), are available (Abbott et al., 2018) and are plotted
403 in the Fig. 3. It is worth pointing out that the HSP values of polymers
404 are notably functions of their molecular weight and degree of crystallinity
405 (Hansen, 2007; Abbott et al., 2018) and the parameters employed here are
406 average values as provided in the HSPiP polymer dataset (Abbott et al.,
407 2018). These polymers may be split into 3 groups based on their HSP: I-in
408 the polar sphere (PVOH), II-in between the spheres (PEG, PLA, PMMA)
409 and III-in the non-polar region (PE and PP). CNC-polymer affinity is not
410 the only factor at play for CNC dispersion in polymer matrices.

411 The protocol employed (melt mixing or solvent casting) has, for instance,
412 a major influence (Bagheriasl et al., 2016, 2017). Assuming that the quality
413 of CNC dispersion in the solvent is important for solvent casting, then other
414 parameters such as the "goodness" of the solvent (Fig. 2), the initial state of
415 CNCs (Beuguel et al., 2018b; Peng et al., 2016) –the use of never-dried, freeze-
416 dried, or spray-dried–, and the protocol employed for the dispersion –such as

417 ultrasonication conditions (Beuguel et al., 2018a)– are also relevant. Keeping
418 these points in mind, it is striking how these polymer-categories (I, II, and
419 III), based solely on HSP, match with the experimental quality reported
420 for the dispersion of sulfuric acid-hydrolyzed CNCs in the aforementioned
421 matrices: PVOH has been reported to be one of the best matrices for CNC
422 dispersion both in solvent casting and melt mixing (Hamad, 2017), which
423 is coherent with it being in the dominant polar sphere of CNCs. A good
424 dispersion of CNCs is also achievable in PLA (Zhang et al., 2015; Bagheriasl
425 et al., 2016, 2017), PEG (Beuguel et al., 2018a; Yao et al., 2017; Zhou et al.,
426 2011; Xu et al., 2013, 2014), and PMMA (Yin et al., 2016) through a solvent
427 casting. Direct melt mixing may however remain difficult for this group II-
428 polymers as in the case of PLA (Raquez et al., 2013; Khoshkava & Kamal,
429 2013; Dhar et al., 2016; Bagheriasl et al., 2017).

430 Dhar et al. (2016) demonstrated that the sulfation of CNC surfaces
431 lessens their dispersibility in PLA matrices, which is consistent with our
432 HSP results: the shift of $\sim +4.6 \text{ MPa}^{1/2}$ in the δ_P of the polar sphere between
433 sulfated CNCs and chemically accessible cellulose increases the distance be-
434 tween the PLA matrices and the (110) and (1 $\bar{1}$ 0) surfaces' sphere from ~ 11.4
435 to $\sim 15.0 \text{ MPa}^{1/2}$. Based on the HSP theory, the absence of any adsorption
436 of PEG on CNC surfaces (Beuguel et al., 2018a; Reid et al., 2017) is also
437 coherent with this polymer being out of any sphere, adsorption being only
438 expected for compounds of very similar HSP (Hansen, 1997). Modification
439 of the nanocrystal OH groups, which is expected to result in a shift of the
440 corresponding surfaces HSP sphere (Peng et al., 2016; Yoo & Youngblood,
441 2016), may significantly improve the CNC dispersion and the reinforcing ef-
442 fect in group II-matrices (Raquez et al., 2013; Yin et al., 2016; Zhang et al.,
443 2015; Khoshkava & Kamal, 2013). It is likely that a systematic HSP char-
444 acterization of the modified CNCs would have concluded that any chemical
445 modification that improves the CNC dispersion in a matrix also reduces
446 the HSP distance between the polar sphere and this matrix, as in the case
447 of Peng et al. (2017). In group III-matrices such as PP (Bagheriasl et al.,
448 2015; Khoshkava & Kamal, 2014) and PE (Lewandowska & Eichhorn, 2016;
449 Inai et al., 2018), nanoscale dispersion in melt compounding seems to be
450 impossible without the use of a compatibilizer. While unmodified nanocrys-
451 tals have an interfacial tension with PP more than fourfold that with PLA,
452 surface modification may, here again, shift the relative affinity of CNCs and
453 make dispersion more favorable in PP with a slightly lower interfacial ten-
454 sion (Khoshkava & Kamal, 2014). Probably due to the low solubility of

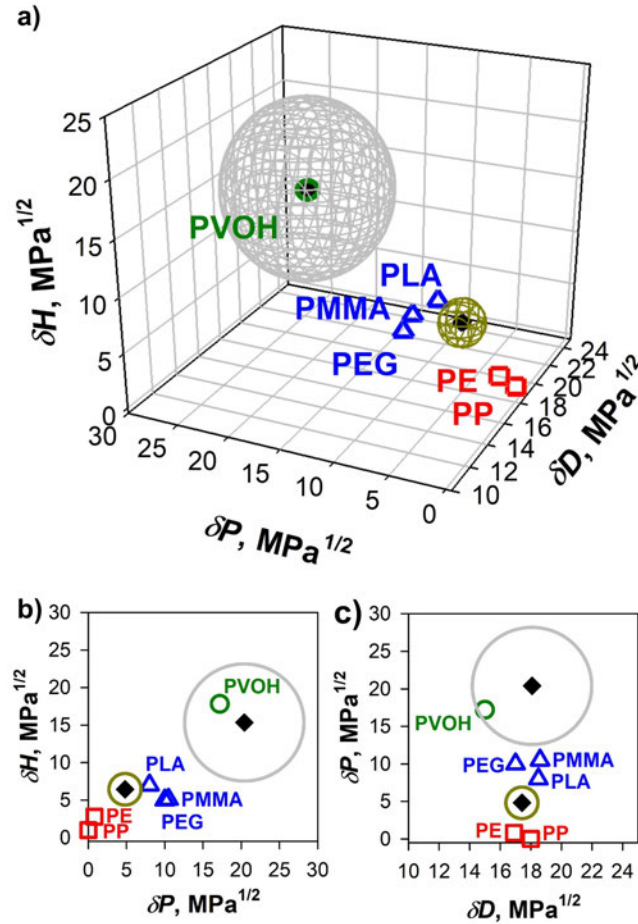


Figure 3: HSP graph of wood-based sulfuric acid hydrolyzed CNCs (see Fig. 2) compared to some commodity polymers. These polymers may be split into 3 groups based on their HSP (Abbott et al., 2018): I-green circles-in the polar sphere for poly(vinyl alcohol) (PVOH); II-blue triangles-in between the spheres for poly(lactic acid) (PLA), poly(ethylene glycol) (PEG), and poly(methyl methacrylate) (PMMA); and III-red squares-in the non-polar region for poly(ethylene) (PE), and poly(propylene) (PP). Categories I, II, and III match, from best to worst, with experimental reports for the dispersibility of CNCs in these matrices. The HSP graph is represented in a 3-dimensional view (a), and in 2-dimensional views alongside the planes δ_H - δ_P (b), and δ_P - δ_D (c).

455 these polymers in common solvents (Hansen, 2007), no experimental data
 456 are available for the solvent casting of these PP and PE nanocomposites.

457 **4. Concluding remarks**

458 In conclusion, we linked CNC dispersibility in a large set of solvents and
459 binary mixtures to the anisotropy of the nanocrystal structure. Wood-based
460 sulfuric acid-hydrolyzed CNCs were found to be predominantly polar par-
461 ticles with a main HSP sphere of radius $7.8 \text{ MPa}^{1/2}$ and of center $(\delta_D ; \delta_P$
462 $; \delta_H) = (18.1; 20.4; 15.3) \pm (0.5; 0.5; 0.4) \text{ MPa}^{1/2}$. This main behavior is
463 thought to reflect the influence of their hydroxyl-rich (110) and $(1\bar{1}0)$ surfaces
464 and is coherent with their behavior described in the literature. While pre-
465 dicted years ago through simulations and expected based on cross-sectional
466 structure analysis of the nanocrystals through X-ray scattering and AFM
467 techniques, this study is the first to experimentally confirm the contribution
468 of **hydrophobic surfaces** to the behavior of CNCs in suspensions. We pro-
469 vide an approximation of their chemical influence through the determination
470 of their Hansen solubility parameters (HSP). Although refinements are still
471 necessary, as based only on two good solvents, the non-polar sphere location
472 is estimated in the range of $(17.4; 4.8; 6.5) \pm (0.3; 0.5; 0.6) \text{ MPa}^{1/2}$ with a
473 radius of $2.1 \text{ MPa}^{1/2}$. This position, relatively to that of the polar sphere, is
474 coherent with results from computer simulations **for the display of (200) lat-**
475 **tice planes by the CNC particles**. Further work is required to determine the
476 influence of the feedstock, of the hydrolysis conditions, and of the dispersion
477 protocol on the display of an amphiphilic behavior by CNCs.

478 HSP graphs are a useful tool to predict the CNC dispersion in polymer
479 matrices and allow us a better understanding of results already published in
480 the literature. Such characterization could be carried out on functionalized
481 particles to understand the effect of the chemical modification on the surface
482 properties of the nanocrystals (Yoo & Youngblood, 2016; Peng et al., 2016)
483 and on their dispersibility (Peng et al., 2017) in non-polar media.

484 **Conflicts of interest**

485 There are no conflicts to declare

486 **Acknowledgments**

487 The authors acknowledge the financial contributions of FPInnovations
488 (Pointe-Claire, QC, Canada), of PRIMA Québec (grant number FPI NCC
489 RD001), of the National Science and Engineering Research Council (NSERC,

490 grant number RDCPJ 490786-15). The Fond de Recherche du Québec - Na-
491 ture et Technologies (FRQNT) kindly provided C. Bruel with a scholarship
492 (number 208324). Cellulforce (Montréal, QC, Canada) is also gratefully ac-
493 knowledged for providing the cellulose nanocrystals. The authors would like
494 to thank Dr. W. Y. Hamad, from FPInnovations, for his contribution in
495 reviewing this work. We are grateful to Dr. Q. Beuguel for his contribution
496 to the TEM and EDX analyses. Finally, Mr. J.-P. Masse is acknowledged
497 for his help with the XRD analysis.

498 References

- 499 Abbott, S. J., Hansen, C. M., & Yamamoto, H. (2018). Hansen solubility
500 parameters in practice software, ebook, datasets. Url: [http://www.hansen-](http://www.hansen-solubility.com)
501 [solubility.com](http://www.hansen-solubility.com), accessed on 2018/07/03.
- 502 Atalla, R. H., & Vanderhart, D. L. (1999). The role of solid state ^{13}C NMR
503 spectroscopy in studies of the nature of native celluloses. *Solid State Nucl.*
504 *Magn. Reson.*, *15*, 1–19.
- 505 Bagheriasl, D., Carreau, P. J., Dubois, C., & Riedl, B. (2015). Proper-
506 ties of polypropylene and polypropylene/poly(ethylene-co-vinyl alcohol)
507 blend/CNC nanocomposites. *Compos. Sci. Technol.*, *117*, 357–363.
- 508 Bagheriasl, D., Carreau, P. J., Riedl, B., Dubois, C., & Hamad, W. Y.
509 (2016). Shear rheology of polylactide (PLA)–cellulose nanocrystal
510 (CNC) nanocomposites. *Cellulose*, *23*, 1885–1897.
- 511 Bagheriasl, D., Safdari, F., Carreau, P. J., Dubois, C., & Riedl, B. (2017).
512 Development of cellulose nanocrystal-reinforced polylactide: A compara-
513 tive study on different preparation methods. *Polym. Compos.*, . DOI:
514 10.1002/pc.24676.
- 515 Beuguel, Q., Tavares, J. R., Carreau, P. J., & Heuzey, M.-C. (2018a). Rheo-
516 logical behavior of cellulose nanocrystal suspensions in polyethylene glycol.
517 *J. Rheol.*, *62*, 607–618.
- 518 Beuguel, Q., Tavares, J. R., Carreau, P. J., & Heuzey, M.-C. (2018b). Ul-
519 trasonication of spray- and freeze-dried cellulose nanocrystals in water. *J.*
520 *Colloid Interface Sci.*, *516*, 23–33.

- 521 Brown, R. M. (1996). The biosynthesis of cellulose. *J. Macromol. Sci., Part*
522 *A: Pure Appl. Chem.*, *A33*, 1345–1373.
- 523 Chaturvedi, K., Ganguly, K., Kulkarni, A. R., Kulkarni, V. H., Nadagouda,
524 M. N., Rudzinski, W. E., & Aminabhavi, T. M. (2011). Cyclodextrin-based
525 siRNA delivery nanocarriers: a state-of-the-art review. *Expert Opin. Drug*
526 *Del.*, *8*, 1455–1468.
- 527 Conley, K. M., Godbout, L., Whitehead, M. A., & van de Ven, T. G. M.
528 (2017a). Reversing the structural chirality of cellulosic nanomaterials. *Cel-*
529 *lulose*, *24*, 5455–5462.
- 530 Conley, K. M., Whitehead, M. A., & van de Ven, T. G. M. (2017b). Prob-
531 ing the structural chirality of crystalline cellulose with induced circular
532 dichroism. *Cellulose*, *24*, 479–486.
- 533 Cousins, S. K., & Brown, R. M. (1995). Cellulose I microfibril assembly:
534 computational molecular mechanics energy analysis favours bonding by
535 van der Waals forces as the initial step in crystallization. *Polymer*, *36*,
536 3885–3888.
- 537 Dhar, P., Bhasney, S. M., Kumar, A., & Katiyar, V. (2016). Acid function-
538 alized cellulose nanocrystals and its effect on mechanical, thermal, crys-
539 tallization and surfaces properties of poly (lactic acid) bionanocomposites
540 films: A comprehensive study. *Polymer*, *101*, 75–92.
- 541 Ding, S.-Y., & Himmel, M. E. (2006). The Maize Primary Cell Wall Mi-
542 crofibril: A New Model Derived from Direct Visualization. *J. Agric. Food*
543 *Chem.*, *54*, 597–606.
- 544 Ding, S.-Y., Liu, Y.-S., Zeng, Y., Himmel, M. E., Baker, J. O., & Bayer,
545 E. A. (2012). How Does Plant Cell Wall Nanoscale Architecture Correlate
546 with Enzymatic Digestibility? *Science*, *338*, 1055–1060.
- 547 Ding, S.-Y., Zhao, S., & Zeng, Y. (2014). Size, shape, and arrangement of
548 native cellulose fibrils in maize cell walls. *Cellulose*, *21*, 863–871.
- 549 Djahedi, C., hle Wohlert, M. B., Berglund, L. A., & Wohlert, J. (2016). Role
550 of hydrogen bonding in cellulose deformation-the leverage effect analyzed
551 by molecular modeling. *Cellulose*, *23*, 2315–2323.

- 552 Dufresne, A. (2017). *Nanocellulose. From Nature to High Performance Tailored Materials*. (2nd ed.). Berlin/Boston: Walter de Gruyter GmbH.
553
- 554 Elazzouzi-Hafraoui, S., Nishiyama, Y., Putaux, J.-L., Heux, L., Dubreuil,
555 F., & Rochas, C. (2008). The shape and size distribution of crystalline
556 nanoparticles prepared by acid hydrolysis of native cellulose. *Biomacromolecules*, *9*, 57–65.
557
- 558 Eyley, S., & Thielemans, W. (2014). Surface modification of cellulose
559 nanocrystals. *Nanoscale*, *6*, 7764–7779.
- 560 French, A. D. (2017). Glucose, not cellobiose, is the repeating unit of cellulose
561 and why that is important. *Cellulose*, *24*, 4605–4609.
- 562 Gardebjer, S., Andersson, M., Engström, J., Restorp, P., Persson, M., &
563 Larsson, A. (2016). Using Hansen solubility parameters to predict the
564 dispersion of nano-particles in polymeric films. *Polym. Chem.*, *7*, 1756–
565 1764.
- 566 Habibi, Y., Lucia, L. A., & Rojas, O. J. (2010). Cellulose Nanocrystals:
567 Chemistry, Self-Assembly, and Applications. *Chem. Rev.*, *110*, 3479–3500.
- 568 Hamad, W. Y. (2017). *Cellulose Nanocrystals Properties, Production and*
569 *Applications*. Chichester, U. K.: Wiley.
- 570 Hamad, W. Y., & Hu, T. Q. (2010). Structure-process-yield interrelation in
571 nanocrystalline cellulose extraction. *Can. J. Chem. Eng.*, *88*, 392–402.
- 572 Hansen, C. M. (1967a). The Three Dimensional Solubility Parameter - Key
573 to Paint Component Affinities I. - Solvents, Plasticizers, Polymers, and
574 Resins. *J. Paint Techn.*, *39*, 104–117.
- 575 Hansen, C. M. (1967b). *The Three Dimensional Solubility Parameter and*
576 *Solvent Diffusion Coefficient, Their Importance in Surface Coating For-*
577 *mulation*. Ph.D. thesis Technical University of Denmark Copenhagen,
578 Denmark.
- 579 Hansen, C. M. (1997). Cohesion Parameters for Surfaces, Pigments, and
580 Fillers. *Surf. Coat. Int.*, *8*, 386–391.
- 581 Hansen, C. M. (2007). *Hansen Solubility Parameters A User's Handbook*.
582 Boca Raton, FL, U. S. A.: CRC Press.

- 583 Hansen, C. M., & Björkman, A. (1998). The Ultrastructure of Wood from a
584 Solubility Parameter Point of View. *Holzforschung*, *52*, 335–344.
- 585 Hansen, C. M., & Skaarup, K. (1967). The Three Dimensional Solubility Pa-
586 rameter - Key to Paint Component Affinities III. - Independent Calculation
587 of the Parameter Components. *J. Paint Techn.*, *39*, 511–514.
- 588 Heiner, A. P., Kuutti, L., & Teleman, O. (1998). Comparison of the interface
589 between water and four surfaces of native crystalline cellulose by molecular
590 dynamics simulations. *Carbohydr. Res.*, *306*, 205–220.
- 591 Hildebrand, J., & Scott, R. L. (1950). *The Solubility of Nonelectrolytes*. (3rd
592 ed.). New York, NY, U. S. A.: Reinhold.
- 593 Hildebrand, J., & Scott, R. L. (1962). *Regular Solutions*. Englewood Cliffs,
594 NJ, U. S. A.: Prentice-Hall.
- 595 Himmel, M. E., Ding, S. Y., Johnson, D. K., Adney, W. S., Nimlos, M. R.,
596 Brady, J. W., & Foust, T. D. (2007). Biomass recalcitrance: engineering
597 plants and enzymes for biofuels production. *Science*, *315*, 804–807.
- 598 Inai, N. H., Lewandowska, A. E., Ghita, O. R., & Eichhorn, S. J. (2018). In-
599 terfaces in polyethylene oxide modified cellulose nanocrystal - polyethylene
600 matrix composites. *Compos. Sci. Technol.*, *154*, 128–135.
- 601 Jarvis, M. (2003). Cellulose stacks up. *Nature*, *426*, 611–612.
- 602 Khoshkava, V., & Kamal, M. R. R. (2013). Effect of Surface Energy on Dis-
603 persion and Mechanical Properties of Polymer/Nanocrystalline Cellulose
604 Nanocomposites. *Biomacromolecules*, *14*, 3155–3163.
- 605 Khoshkava, V., & Kamal, M. R. R. (2014). Effect of drying conditions on cel-
606 lulose nanocrystal (cnc) agglomerate porosity and dispersibility in polymer
607 nanocomposites. *Powder Technol.*, *261*, 288–298.
- 608 Kronberg, B., Holmberg, K., & Lindman, B. (2014). *Surface Chemistry of*
609 *Surfactants and Polymers*. (1st ed.). Chichester, U. K.: Wiley.
- 610 Kuutti, L., Peltonen, J., Pere, J., & Teleman, O. (1995). Identification and
611 surface structure of crystalline cellulose studied by atomic force microscopy.
612 *J. Microsc.-Oxford*, *178*, 1–6.

- 613 Larsson, A., & Johns, W. E. (1988). Acid-base interactions between cell-
614 lose/lignocellulose and organic molecules. *J. Adhesion*, *25*, 121–131.
- 615 Lewandowska, A. E., & Eichhorn, S. J. (2016). Raman imaging as a tool for
616 assessing the degree of mixing and the interface between polyethylene and
617 cellulose nanocrystals. *IOP Conf. Ser. Mater. Sci. Eng.*, *139*, 012030.
- 618 Li, Q., & Renneckar, S. (2011). Supramolecular Structure Characterization
619 of Molecularly Thin Cellulose I Nanoparticles. *Biomacromolecules*, *12*,
620 650–659.
- 621 Liu, D., Chen, X., Y.Yue, Chen, M., & Wu, Q. (2011). Structure and rheology
622 of nanocrystalline cellulose. *Carbohydr. Polym.*, *84*, 311–322.
- 623 Machui, F., Langner, S., Zhu, X., Abbott, S., & Brabec, C. J. (2012). *Sol.*
624 *Energ. Mat. Sol. C.*, *100*, 138–146.
- 625 Marques, H. M. C. (2010). A review on cyclodextrin encapsulation of essential
626 oils and volatiles. *Flavour Frag. J.*, *25*, 313–326.
- 627 Matthews, J. F., Skopec, C. E., Mason, P. E., Zuccato, P., Torget, R. W.,
628 Sugiyama, J., Himmel, H. E., & Brady, J. W. (2006). Computer simulation
629 studies of microcrystalline cellulose I β . *Carbohydr. Res.*, *341*, 138–152.
- 630 Mazeau, K., & Rivet, A. (2008). Wetting the (110) and (100) Surfaces of I β
631 Cellulose Studied by Molecular Dynamics. *Biomacromolecules*, *9*, 1352–
632 1354.
- 633 Mazeau, K., & Wyszomirski, M. (2012). Modelling of Congo red adsorption
634 on the hydrophobic surface of cellulose using molecular dynamics. *Cellu-*
635 *lose*, *19*, 1495–1506.
- 636 Medronho, B., Romano, A., Miguel, M. G., Stigsson, L., & Lindman, B.
637 (2012). Rationalizing cellulose (in)solubility: reviewing basic physicochem-
638 ical aspects and role of hydrophobic interactions. *Cellulose*, *19*, 581–587.
- 639 Minhas, P. S., & Robertson, A. A. (1967). Accessibility of Cellulose by the
640 Thallous Ethylate Method-Application to the Measurement of Cellulose
641 Liquid Interactions 1. *Textile Res. J.*, *37*, 400–408.

- 642 Moon, R. J., Martini, A., Nairn, J., Simonsen, J., & Youngblood, J. (2011).
643 Cellulose nanomaterials review: structure, properties and nanocomposites.
644 *Chem. Soc. Rev.*, *40*, 3941–3994.
- 645 Nishiyama, Y. (2017). Molecular interactions in nanocellulose assembly. *Phil.*
646 *Trans. R. Soc. A.*, *376*, 20170047.
- 647 Nishiyama, Y., Langan, P., & Chanzy, H. (2002). Crystal Structure and
648 Hydrogen-Bonding System in Cellulose I $_{\beta}$ from Synchrotron X-ray and
649 Neutron Fiber Diffraction. *J. Am. Chem. Soc.*, *124*, 9074–9082.
- 650 Nishiyama, Y., Sugiyama, J., Chanzy, H., & Langan, P. (2003). Crystal
651 Structure and Hydrogen Bonding System in Cellulose I $_{\alpha}$ from Synchrotron
652 X-ray and Neutron Fiber Diffraction. *J. Am. Chem. Soc.*, *125*, 14300–
653 14306.
- 654 Peng, S. X., Chang, H., Kumar, S., Moon, R. J., & Youngblood, J. P. (2016).
655 A comparative guide to controlled hydrophobization of cellulose nanocrystals
656 via surface esterification. *Cellulose*, *23*, 1825–1846.
- 657 Peng, S. X., Shrestha, S., Yoo, Y., & Youngblood, J. P. (2017). Enhanced
658 dispersion and properties of a two-component epoxy nanocomposite using
659 surface modified cellulose nanocrystals. *Polymer*, *112*, 359–368.
- 660 Petersson, L., Kvien, I., & Oksman, K. (2007). Structure and thermal properties
661 of poly(lactic acid)/cellulose whiskers nanocomposite materials. *Compos. Sci. Technol.*, *67*, 2535–2544.
- 663 Raquez, J.-M., Habibi, Y., Murariu, M., & Dubois, P. (2013). Polylactide
664 (PLA)-based nanocomposites. *Prog. Polym. Sci.*, *38*, 1504–1542.
- 665 Reid, M. S., Villalobos, M., & Cranston, E. D. (2017). The role of hydrogen
666 bonding in non-ionic polymer adsorption to cellulose nanocrystals and
667 silica colloids. *Curr. Opin. Colloid In.*, *29*, 76–82.
- 668 Sèbe, G., Ham-Pichavant, F., Ibarboure, E., Koffi, A. L. C., & Tingaut,
669 P. (2012). Supramolecular Structure Characterization of Cellulose II
670 Nanowhiskers Produced by Acid Hydrolysis of Cellulose I Substrates.
671 *Biomacromolecules*, *13*, 570–578.

- 672 Segal, L., Creely, J. J., Martin, Jr, A. E., & Conrad, C. M. (1959). An
673 Empirical Method for Estimating the Degree of Crystallinity of Native
674 Cellulose Using the X-Ray Diffractometer. *Text. Res.*, *29*, 786–794.
- 675 Siqueira, G., Bras, J., & Dufresne, A. (2010). New Process of Chemical Graft-
676 ing of Cellulose Nanoparticles with a Long Chain Isocyanate. *Langmuir*,
677 *26*, 402–411.
- 678 Sojoudiasli, H., Heuzey, M.-C., Carreau, P. J., & Riedl, B. (2017). Rheologi-
679 cal behavior of suspensions of modified and unmodified cellulose nanocrys-
680 tals in dimethyl sulfoxide. *Rheol. Acta*, *56*, 673–682.
- 681 Stefanis, E., & Panayiotou, C. (2008). Prediction of Hansen Solubility Pa-
682 rameters with a New Group-Contribution Method. *Int. J. Thermophys.*,
683 *29*, 568–585.
- 684 Uhlig, M., Fall, A., Wellert, S., Lehmann, M., Prévost, S., Wågberg, L.,
685 von Klitzing, R., & Nyström, G. (2016). Two-dimensional aggregation and
686 semidilute ordering in cellulose nanocrystals. *Langmuir*, *32*, 442–450.
- 687 Usov, I., Nyström, G., Adamcik, J., Handschin, S., Schütz, C., Fall, A.,
688 Bergström, L., & Mezzenga, R. (2015). Understanding nanocellulose chi-
689 rality and structure–properties relationship at the single fibril level. *Nat.*
690 *Commun.*, *6*, 7564.
- 691 Wade, R. H., & Creely, J. J. (1974). Structure and Stability of Chloroform-
692 Included Cotton Cellulose. *Text. Res. J.*, *44*, 941–945.
- 693 Xu, X., Liu, F., Jiang, L., Zhu, J. Y., Haagensohn, D., & Wiesenborn, D. P.
694 (2013). Cellulose Nanocrystals vs. Cellulose Nanofibrils: A Compara-
695 tive Study on Their Microstructures and Effects as Polymer Reinforcing
696 Agents. *ACS Appl. Mater. Inter.*, *5*, 2999–3009.
- 697 Xu, X., Wang, H., Jiang, L., Wang, X., Payne, S. A., Zhu, J. Y., & Li, R.
698 (2014). Comparison between Cellulose Nanocrystal and Cellulose Nanofib-
699 ril Reinforced Poly(ethylene oxide) Nanofibers and Their Novel Shish-
700 Kebab-Like Crystalline Structures. *Macromolecules*, *47*, 3409–3416.
- 701 Yamane, C., Aoyagi, T., Ago, M., Sato, K., Okajima, K., & Takahashi, T.
702 (2006). Two different surface properties of regenerated cellulose due to
703 structural anisotropy. *Polym. J.*, *38*, 819–826.

- 704 Yao, K., Meng, Q., Bulone, V., & Zhou, Q. (2017). Flexible and Respon-
705 sive Chiral Nematic Cellulose Nanocrystal/Poly(ethylene glycol) Compos-
706 ite Films with Uniform and Tunable Structural Color. *Adv. Mater.*, *29*,
707 1701323.
- 708 Yin, Y., Tian, X., Jiang, X., Wang, H., & Gao, W. (2016). Modification
709 of cellulose nanocrystal via SI-ATRP of styrene and the mechanism of its
710 reinforcement of polymethylmethacrylate. *Carbohydr. Polym.*, *142*, 206–
711 212.
- 712 Yoo, Y., & Youngblood, J. P. (2016). Green One-Pot Synthesis of Surface
713 Hydrophobized Cellulose Nanocrystals in Aqueous Medium. *ACS Sustain-
714 able Chem. Eng.*, *4*, 3927–3938.
- 715 Yu, H., & Qin, Z. (2012). Effect of Cellulose nanocrystal on Crystallization
716 Behavior of Poly(3- β -hydroxybutyrate- β -5-hydroxyvalerate).
717 *Adv. Mat. Res.*, *430-432*, 20–23.
- 718 Yu, H.-Y., Qin, Z.-Y., Liu, Y.-N., Chen, L., Liu, N., & Zhou, Z. (2012).
719 Simultaneous improvement of mechanical properties and thermal stability
720 of bacterial polyester by cellulose nanocrystals. *Carbohydr. Polym.*, *89*,
721 971–978.
- 722 Zhang, C., Salick, M. R., Cordie, T. M., Ellingham, T., Dan, Y., & Turng, L.-
723 S. (2015). Incorporation of poly(ethylene glycol) grafted cellulose nanocrys-
724 tals in poly(lactic acid) electrospun nanocomposite fibers as potential scaf-
725 folds for bone tissue engineering. *Mater. Sci. Eng. C Mater. Biol. Appl.*,
726 *49*, 463–471.
- 727 Zhou, C., Chu, R., Wu, R., & Wu, Q. (2011). Electrospun polyethylene
728 oxide/cellulose nanocrystal composite nanofibrous mats with homogeneous
729 and heterogeneous microstructures. *Biomacromolecules*, *12*, 2617–2625.